Supplementary Materials

Cloning of decoy plasmids. All decoy plasmids were cloned into pRG475 that contains P_{tet}-*cfp*, a pUC18 based replication origin (pMB1 derivative) and P_{BAD}-*rop* that reduces the plasmid copy number. To facilitate decoy binding site cloning, two *Bsa*I sites were introduced with GGTC and GCTT overhangs after digestion. Two oligonucleotides, PhoBsite-S and PhoBsite-R, were annealed to create a DNA fragment containing the consensus PhoB-binding site (yellow shaded) and two overhangs complementary to GGTC and GCTT overhangs from pRG475. The annealed oligos were treated with T4 kinase and added into the Golden Gate reaction mixture to clone pRG491 (1 consensus site).

PhoBsite-S: 5′-**GACC**CGGGGAGGGTCGTT CTGTCATAAAACTGTCATATTC CACCGGGAAG -3′
PhoBsite-R: 3′- GCCCCTCCCAGCAA GACAGTATTTTGACAGTATAAG GTGGCCCTTC**CGAA**-5′

Cooperative binding to multiple binding site repeats could occur for binding sites immediately adjacent to each other. To minimize potential cooperative binding to decoy site repeats, the consensus PhoB-binding site is flanked by non-specific bases that allow ~28 bp spacing between the assembled repeats of consensus sites. To generate multiple repeats of PhoB decoy sites, two additional primers PhoBsite-S3 and PhoBsite-R3 were combined with -S and -R primers to generate fragments with different combinations of overhangs. DNA fragments SR3 and S3R together with pRG475 were used to clone pRG492 (2 consensus sites). Another fragment S3R3, capable of self-ligating, were combined with SR3 and S3R to generate multiple repeats, eventually yielding pLH6 (3 consensus sites).

SR3:
PhoBsite-S: 5′-**GACC**CGGGGAGGGTCGTT CTGTCATAAAACTGTCATATTC CACCGGGAAG -3′
PhoBsite-R3: 3′- GCCCCTCCCAGCAA GACAGTATTTTGACAGTATAAG GTGGCCCTTC**GTCC**-5′

S3R3:
PhoBsite-S3: 5′-**CAGG**CGGGGAGGGTCGTT CTGTCATAAAACTGTCATATTC CACCGGGAAG -3′

PhoBsite-R3: 3′- GCCCCTCCCAGCAA GACAGTATTTTGACAGTATAAG GTGGCCCTTCGTCC-5′

S3R:
PhoBsite-S3: 5′-CAGGCGGGGAGGGTCGTT CTGTCATAAAACTGTCATATTC CACCGGGAAG -3′
PhoBsite-R: 3′- GCCCCTCCCAGCAA GACAGTATTTTGACAGTATAAG GTGGCCCTTCCGAA-5′

To make decoy plasmids with higher number of consensus sites, the DNA fragment with multiple decoy sites was used as template and the following primers: RGn-15f, GCTGGTCTCT GACCATGCTGACCCGGGGAGGG; RGn-16r, GCTCGTCTCT AAGCAGCTCAAGC CTTCCCGGT; and RGn-16rb, GCT GGTCTCT GGTCAGCTCAAGC CTTCCCGGT, were used to generate DNA fragments with different combinations of overhangs, eventually yielding pLH8 (5 concensus sites) and pLH9 (7 consensus sites). The following gBlock DNA fragment was ordered from IDT and cloned into pRG475 to create pLH10 (0 concensus site).

gBlock DNA (0 site)
GTAATGGTCTCTGACCATGCTGACCCGGGGAGGGTCGTTCGAGACGGCAGGCCCGA
ACGCGAACCACCGGGAAGCAGGCGCCGACCGTCGTTGCCGTTCCGGTTTGGCTGGT
CGCACGCCGAAGCGGAGAAGCGTCGTTCCGCAAGGCCGAACCGACGTCTCGACCGG
GAAGGCTTGAGCTGCTTAGAGACCAACTA

Determination of binding affinity of the decoy site. PhoB-binding affinity of the decoy site was determined by electrophoretic mobility shift assays (EMSA) similarly as other PhoB-binding sites within the *phoA*, *phoB* and *phnC* promoters (1,2). Fluorescent DNA fragments were prepared by PCR using primers labeled with 5'-fluorescein. Plasmid pRG491 (1 site) was used as template for the decoy site and pLH10 (0 site) as the template for a negative control. Sequences for the two are listed below:

Decoy DNA (1 site):
atcacatggtcctgctggagttcgtgaccgccgccgggatcactctcggcatggacgagctgtacaagtagctgacCCGGGGAGG
GTCGTT**CTGTCATAAAACTGTCATATTC**CACCGGGAAGgcttgagctcctagatacattcaaatatgta
tccgctcatgagacaataaccctgata

Control DNA (0 site):

atcacatggtcctgctggagttcgtgaccgccgccgggatcactctcggcatggacgagctgtacaagtagctgacCATGCTGAC
CCGGGGAGGGTCGTTCGAGACGGCAGGCCCGAACGCGAACCACCGGGAAGCAGGC
GCCGACCGTCGTTGCCGTTCCGGTTTGGCTGGTCGCACGCCGAAGCGGAGAAGCGTC
GTTCCGCAAGGCCGAACCGACGTCTCGACCGGGAAGGCTTGAGCTgcttgagctcctagataca
ttcaaatatgtatccgctcatgagacaataaccctgata

EMSA assays were performed with phosphorylated PhoB as described (1). Protein-DNA mixtures were analyzed by 10% TBE gels (130 v, 50 min on ice) and imaged by fluorescence imaging using a FluorChem Q (Alpha Innotech). The fraction of PhoB-bound DNA was calculated based on relative DNA band intensities quantified with ImageJ (NIH). Fractions of PhoBp bound to DNA were subtracted from total PhoBp concentrations to yield free unbound PhoBp concentrations to plot the binding curve. The binding curves were fitted with the Hill equation to derive the dissociation constant K_D. Previous affinity determination of *phnC* binding site used the total PhoBp concentration instead of free PhoBp concentration for fitting (2), thus the *phnC* EMSA data were re-analyzed to give the affinity K_D of 1.5 μM.

Determination of plasmid copy number by qPCR. Four primer sets were chosen to amplify fragments of similar length from three chromosomal genes: *dxs*, *secD*, and *tdk*, as well as one plasmid-borne gene: *bla*. The relative DNA amount ratio of *bla* to *dxs* represent the plasmid copy number while *secD* and *tdk* are controls with an expected copy number of 1. In order to minimize potential amplification differences due to PCR product size, all primer sets were designed to amplify an ~120 bp fragment. Sequences of primers are listed below:

bla-f: GGGTTACATCGAACTGGATCTC
dxs-f: CGTCCTGATATGCTGGTGATT
secD-f: GTATCGCGGGTATCGTCTTAAC
tdk-f: CGGGTAAGTCTACAGCATTGT

bla-r: GGCGTCAACACGGGATAATA
dxs-r: TCGCGCAGTGAAGAGTAAAG
secD-r: CGCCACGATAACCTTCATCA
tdk-r: ACCTATACGCGAACTGACTTTC

Amplification efficiency was evaluated for *bla* and *dxs*. Extracted DNA from RU2079/pLH10 was diluted to final concentrations of 30, 15, 7.5, 3.75, and 1.875 ng/µL, and added to qPCR reaction mix with the following recipe: 10 µL GoTaq 2x mix, 1.5 µL of each primer (7.5 pmol each), 6 µL nuclease-free water, and 1 µL of the template DNA. Mean C_t values of three replicates at each concentration were calculated and plotted against the logarithm of respective template DNA concentrations. The linearly fitted slopes represent the amplification efficiency. a value of ~1 indicates a doubling of the PCR product per cycle.

To determine the relative amount of the target gene compared to the reference gene, differences in C_t values between the target gene and *dxs*, ΔC_t, were calculated by subtracting the averaged C_t value of three replicates of the *dxs* gene from the C_t value of each corresponding sample well. Plasmid copy number was calculated from four independent DNA extractions of RU2079/pLH10. Effects of decoy number or hosting strain background on plasmid copy number were evaluated by comparing ΔC_t values of samples of interest to ΔC_t of RU2079/pLH10. Two template concentrations, 30 and 3.75 ng/µL, with three replicates each concentration were used each sample to calculate the ΔC_t difference, $\Delta\Delta C_t$. The relative ratio of plasmid copy number was calculated by $2^{\wedge}\Delta\Delta C_t$.

Assessing the relative abundance of TF to TFBS. Total numbers of TFBSs for *E. coli* TFs were obtained from regulonDB (3) (link, http://regulondb.ccg.unam.mx/search?term=regulon&organism=ECK12&type=All). These TFBSs are curated by regulonDB according to multiple criteria and are designated as TFBSs from the experimental dataset. Absolute protein copies of TFs from the above regulonDB list were extracted from Table S6 of the published proteome study (4). Among the 22 growth conditions reported, three stress related conditions including

stationary phase 1 day, stationary phase 3 days and osmotic stress were excluded. Protein copies across the remaining 19 conditions were used to calculate the median and range of TF abundance shown in Figure 6A. TF proteins with measurement confidence scores below the arbitrary value of 50 were excluded, leaving a total of 119 TFs with both abundance and TFBS data (Table S3). Specifically, for PhoB, mass spec measurements of PhoB have a low confidence score of ~36, one of the lowest among TFs, thus are excluded from the global analyses shown in Figure 6. PhoB abundance is estimated based on our previous analyses with quantitative immunoblotting (5).

TFBS data from high throughput (HT) experiments have been curated in the HT datasets of regulonDB (link, http://regulondb.ccg.unam.mx/highthroughputdatasetssearch?term=all). TFs with ChIP (ChIP, ChIP-seq, and ChIP-exo) or gSELEX binding studies were selected. For each HT dataset, the total number of binding site entries was considered as the number of TFBSs. If there are multiple HT datasets for one single TF, the median number of TFBSs was used to represent the total number of TFBSs from HT datasets for that particular TF, which was then compared to the number of TFBSs from the experimental dataset to calculate the ratio shown in Figure 6B.

Modeling of autoregulation kinetics. PhoB phosphorylation and protein expression occur with a time scale much longer than the fast DNA binding reactions. Quasi-equilibrium approximation is used for competitive DNA binding reactions, and only the phosphorylation and protein expression kinetics are considered. PhoB phosphorylation kinetics are approximated using the following equation with a half-time t_p:

$$\frac{d[RRp]_T}{dt} = \frac{1}{t_p}\left(-[RRp]_T + \underbrace{\frac{1}{2}\left(C_p + C_t + [RR]_T\right) - \frac{1}{2}\sqrt{(C_p + C_t + [RR]_T)^2 - 4C_p[RR]_T}}\right). \quad [S1]$$

The indicated term within the parentheses ensures the steady state phosphorylation level satisfying eq. 1 in the main text.

Three schemes with increasing complexity have been modeled for autoregulatory expression of the RR PhoB (Figure S6). The first scheme has a sole positive feedback through an activation site with the affinity of K_B within the autoregulatory promoter (Figure S6A). This is a basic autoregulation mechanism identified in many two-component systems and other transcription factors. PhoB protein production rate, RatePF, is dependent on occupancy of the activation site:

$$\frac{d[RR]_T}{dt} = \underbrace{P_0\left(1 + P_1\frac{[RRp]_{free}^2}{[RRp]_{free}^2 + K_B^2}\right)}_{RatePF} - k_{dil}[RR]_T. \quad [S2a]$$

It has been shown that PhoB autoregulation also contains a coupled negative feedback via a second repression site with the affinity K_{rp} (2). Occupancy of this weak site repress PhoB expression, thus a repression factor can be used to modify the protein production rate RatePF:

$$\frac{d[RR]_T}{dt} = \underbrace{RatePF * (1 - \frac{[RRp]_{free}^2}{[RRp]_{free}^2 + K_{rp}^2})}_{RateCF} - k_{dil}[RR]_T. \quad [S2b]$$

Pi starvation is known to elicit stress response that alters both protein production rate and growth rate. An extremely simplified model is adopted for simulating stress-induced repression effect. It is assumed that protein production undergoes the same repression as growth rate so that the repression function *f(t)* can be derived from the observed growth rate change. The protein production rate RateCF and growth dilution rate k_{dil} are further modified by *f(t)*:

$$\frac{d[RR]_T}{dt} = f(t) * RateCF - f(t)k_{dil}[RR]_T. \quad [S2c]$$

$$f(t) = b + (1-b)\frac{1}{1+e^{k(t-t_s)}} \quad [S3]$$

To simulate kinetics of $[RR]_T$ and $[RRp]_T$ for three autoregulation schemes, eqs. 1, S1 and S2 are combined for ODE simulation with the following initial concentrations: $[RR]_T$ = 0.45 μM, $[RRp]_T$=0.

Kinetic parameter estimation. Parameter values are estimated from experimental results and all parameter values are listed in Table S2. For the phosphorylation module, values of the composite parameters C_p and C_t are derived from previous cellular phosphorylation profiling of PhoB (5). Original values are based on pmol per 0.3 O.D. of cell, a cell volume of $1x10^{-15}$ l and an O.D. of 10^9 cells are used to convert the units to μM. The phosphorylation half-time t_p is estimated based on cellular phosphorylation kinetics at multiple $[PhoB]_T$ levels (2).

Binding of PhoBp to the YFP reporter site, endogenous chromosomal binding sites, plasmid-borne decoy sites and the sites within the autoregulatory *phoB* promoter are modeled with competitive binding equilibria with affinities K_r, K_{en}, K_{decoy}, K_B and K_{rp}, respectively. Except for K_{en}, DNA binding affinities to various sites are obtained from *in vitro* EMSA binding studies. All the endogenous chromosomal binding sites are treated as a group of sites with a single affinity K_{en} for simplicity. The total number of sites, En0, is derived from the ChIP-chip study of genome-wide PhoB binding pattern (6). Information contents of binding sites are believed to reflect their affinities for biochemically confirmed PhoB sites (1). The median

information content of these sites is found to be close to the information content of *phoA* site, thus the affinity value of the *phoA* site, 0.6 μM, is used for K_{en}.

Concentrations of different DNA binding sites can be calculated by multiplying the number of DNA sites with the concentration of a single DNA site, DNA_0, and the copy number of genome equivalents. DNA_0 is based on one site in a cell volume of $1x10^{-15}$ l. Because decoy plasmid copy number was measured by qPCR using the *dxs* gene as reference and locations of *phoB* and the reporter gene are not distant from *dxs*, the copy number of *dxs* is used as the genome equivalent. Gene copy number is dependent on growth rates and the gene location relative to the chromosomal replication origin. The following formula is used to calculate *dxs* copy number:

$$gene\ copy = 2^{(C*(1-m')+D)/\tau},$$

in which τ is the doubling time (~108 min) calculated from growth curves shown in Figure S6, *m'* is the relative distance (0.5) of *dxs* to the replication origin oriC, C (67 min) and D (30 min) is growth-dependent times of different replication phases (7).

PhoB protein concentrations before and after Pi starvation are from previous quantification from immunoblots (5). As described previously (2), autoregulation parameters P_0 and P_1 care calculated from steady state solutions of eq. S2a or S2b based on PhoB concentrations before and after Pi starvation. To derived parameters for stress function *f(t)*, O.D. measurements were converted to growth rates (Figure S6H) and fitted with the indicated function.

Fig. S1

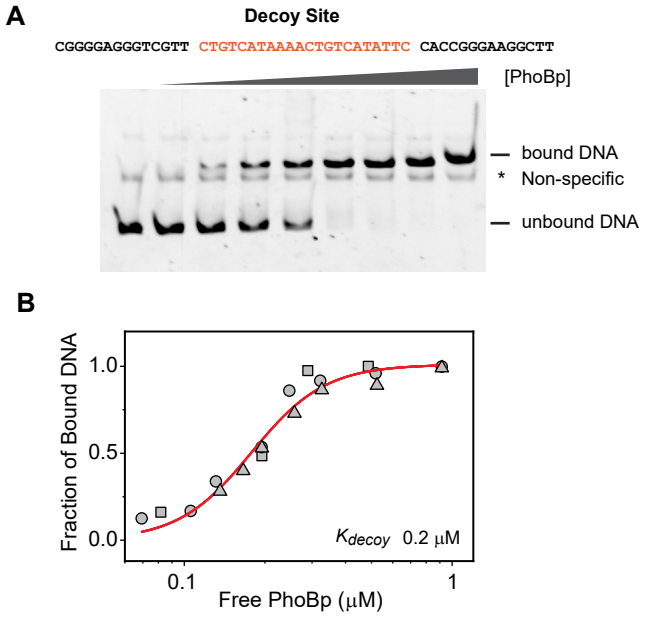

Figure S1. Determination of the binding affinity of decoy to PhoBp with EMSA. (**A**) Binding of PhoBp to the decoy DNA. Each decoy site contains a 22 bp consensus PhoBp binding site (highlighted in *red*) and two 14 bp non-specific sequence flanked at both ends. For the representative gel shown here, EMSA was done using 0.04 μM of DNA containing a single decoy site in the presence of 0, 0.08, 0.12, 0.16, 0.24, 0.32, 0.4, 0.6, 1 μM of PhoB~P. (**B**) Determination of the binding affinity. Fractions of bound DNA were quantified from EMSA gel images. Data from three independent experiments are shown in squares, circles and triangles. The red line indicates the curve fitted with a Hill equation and the resulting affinity is 0.2 μM.

Fig. S2

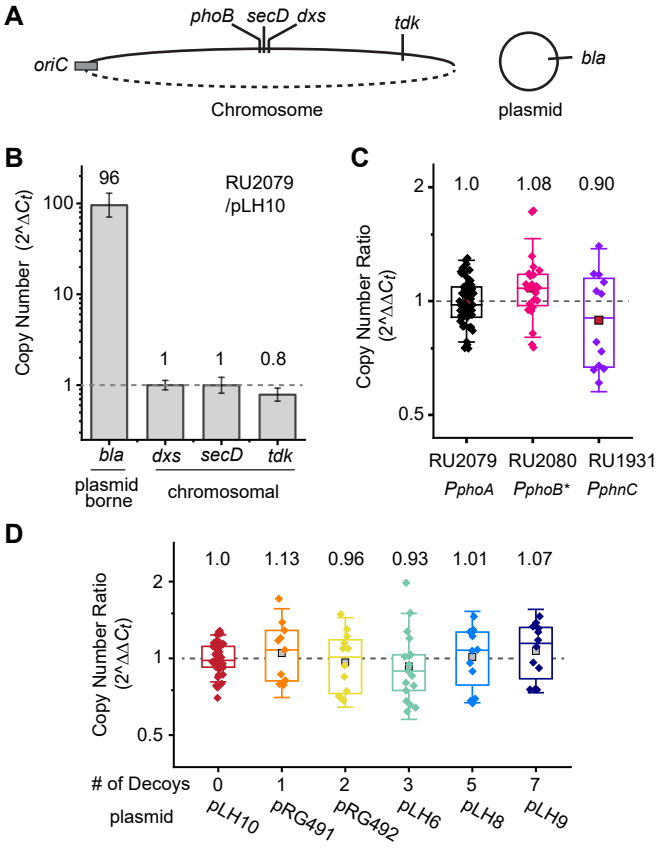

Figure S2. Determination of the plasmid copy number by qPCR. (**A**) Schematic diagram of qPCR markers. The relative DNA amount of the plasmid-borne *bla* gene to the chromosomal reference gene *dxs* was measured by qPCR. Two additional chromosomal genes, *secD* and *tdk*, were included as controls. Genomic positions of these genes in relation to the replication origin (*oriC*) were illustrated. (**B**) Quantification of the plasmid copy number. Difference between threshold cycles of indicated genes and the reference gene *dxs*, ΔC_t, was used to calculate the copy number. DNA copy numbers are indicated at top of the bars and the copy number of the decoy control plasmid pLH10 is 96 ± 31. The two other chromosomal control genes, *secD* and *tdk*, showed similar copy number of 1 as *dxs*, validating the qPCR method for copy number determination. Data are shown as mean ± SD. DNA samples were extracted from RU2079/pLH10. The number of biologically independent samples are: N=4, for *bla* and *dxs*; N=2, for *secD* and *tdk*, and each sample was diluted to five concentrations with at least two replicates each concentration for ΔC_t measurement. (**C**) Quantification of the relative copy number of pLH10 in three different reporter strains. Differences between ΔC_t of the indicated strain and RU2079/pLH10 ($\Delta\Delta C_t$) were used to calculate the relative copy number ratio. pLH10 has similar copy numbers in RU2080 and RU1931 as in RU2079, with the ratio close to 1. (**D**) Quantification of the relative copy number of different decoy plasmids in strain RU2079. DNA sample of RU2079/pLH10 was used as a reference to calculate $\Delta\Delta C_t$ for strains containing indicated decoy plasmids. All decoy plasmids have similar copy numbers as pLH10. Box plots in C and D indicate the median (horizontal bar in the middle), mean (square), standard deviation (whisker) and individual qPCR measurement (diamond). Taken together, strain background or different number of decoy repeats do not alter the plasmid copy number greatly. Thus, the total number of decoy sites are calculated by multiplying the plasmid copy number 96 with the number of decoy repeats, resulting in the following numbers, 0 (pLH10), 96 (pRG491), 198 (pRG492), 288 (pLH6), 480 (pLH8) and 672 (pLH9).

Fig. S3

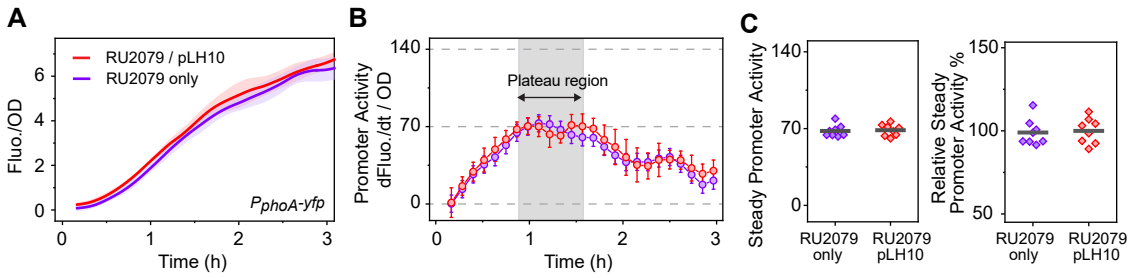

Figure S3. Identical reporter activation profiles between strains with or without pLH10. (**A**) Time courses of P_{phoA}-*yfp* activation in RU2079 and RU2079/pLH10. Plasmid pLH10 contains the same plasmid backbone as other decoy-harboring plasmids but no PhoB-binding site. The presence of pLH10 did not impact the P_{phoA}-*yfp* fluorescence activation profile. Solid lines and the corresponding shaded ranges indicate the mean and SD. (**B**) Calculation of the plateaued promoter activity. OD-normalized first derivatives of culture fluorescence were calculated to represent the promoter activity. Data are shown as mean ± SD from eight individual culture wells. Because it has been shown that stress response reduces the promoter activity during the late stage of phosphate starvation (8), a plateaued region of promoter activities (gray shaded) before the transcription repression by stress was identified, and the average of promoter activities within this region was considered as transcription output. (**C**) Comparison of steady promoter activities between RU2079 and RU2079/pLH10. Steady promoter activities (*left*) were used to calculate the relative promoter activities (*right*) by dividing the average promoter activities of the reference strain RU2079/pLH10. Diamonds illustrate the steady promoter activity of individual culture well and horizontal bars indicate the mean.

Fig. S4

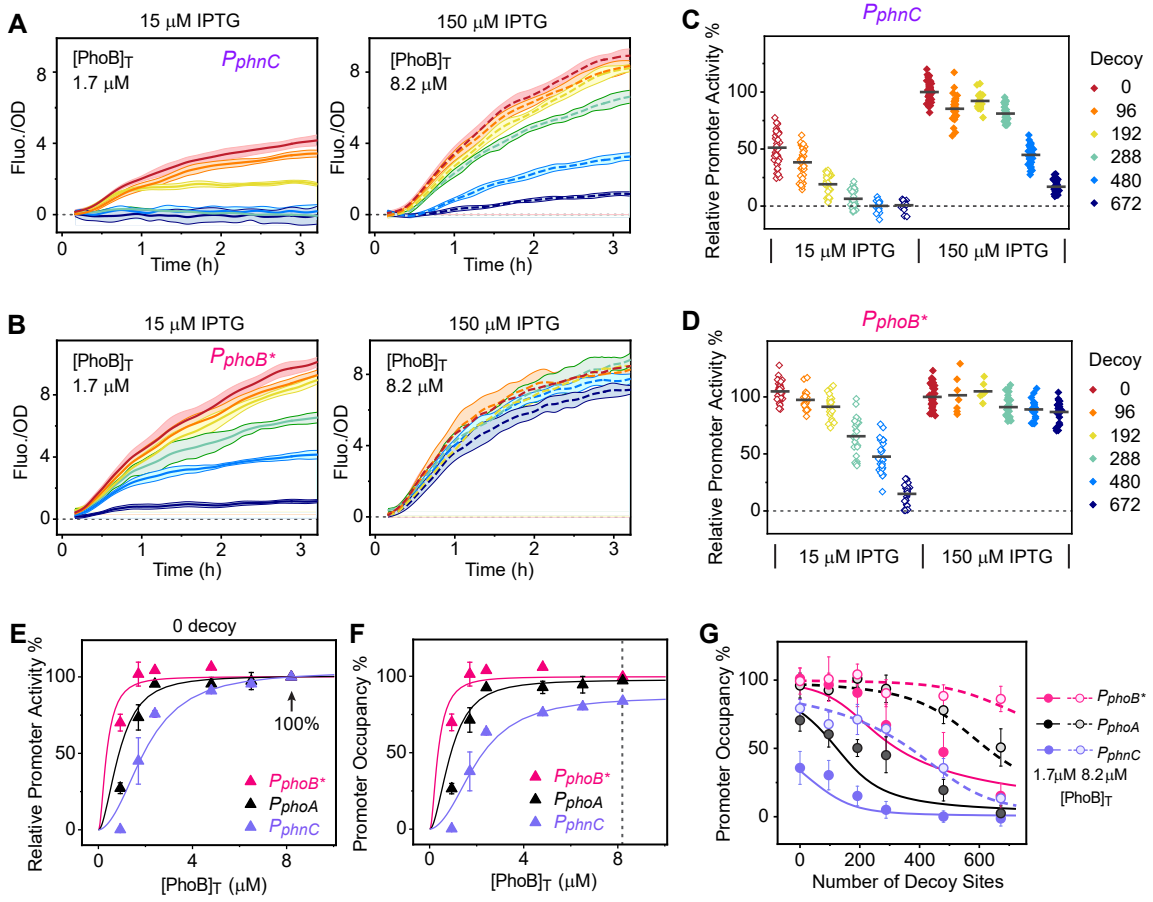

Figure S4. Effects of decoy sites on transcription output in engineered non-autoregulatory strains. (**A** and **B**) Time courses of P_{phnC}-*yfp* activation in RU1990 (**A**) and P_{phoB*}-*yfp* activation in RU1989 (**B**) in the presence of 15 μM (*left*) and 150 μM (*right*) IPTG. Lines with corresponding shaded ranges indicate mean ± SD from 8 individual wells for each decoy plasmid. (**C**-**D**) Decrease of relative steady promoter activities by increasing number of decoy sites. Steady promoter activities were calculated as described in Figure S3 and compared against that of the corresponding strain carrying pLH10 (0 decoy) with constant PhoB expression at 150 μM IPTG. The resulting relative steady promoter activities are shown for reporter strains RU1990 P_{phnC}-*yfp* (**C**) and RU1989 P_{phoB*}-*yfp* (**D**). Diamond symbols illustrate data from individual wells in the presence of 15 μM (open) and 150 μM IPTG (solid). Horizontal bars indicate the averages. At least two independent experiments with eight individual cultures per experiment were performed to obtain the data shown. (**E**-**G**) Comparison of the relative promoter activities to the modeled curves. Relative promoter activities were also obtained for three reporter strains carrying 0 decoy site (pLH10) at the following IPTG concentrations, 5, 15, 25, 50, 75 and 150 μM IPTG (**E**) with corresponding PhoB concentrations at 0.93, 1.7, 2.4, 4.8, 6.5 and 8.2 μM (1). Promoter occupancy data at varying $[RR]_T$ levels were simulated (**F**). It has been shown that RR phosphorylation saturates at a level of C_p (9). At the saturated PhoBp level around 4 μM (5), promoter occupancy of P_{phnC} does not reach 100% and plateaus around 80%. For comparison to experimental data, either promoter occupancy curves need to be converted to relative promoter activities (solid lines in **E**) or the measured relative promoter activities need to be converted to promoter occupancy (triangles in **F**). To make such conversion, modeled occupancy at 150 μM IPTG in the absence of decoy (indicated by the vertical dashed line in **F**) was considered as a reference. Dividing the modeled promoter occupancy values by the corresponding references for respective promoters resulted in the modeled relative promoter activities while multiplying the relative promoter activities with the reference occupancy yielded promoter occupancy data. Relative promoter activities in Figure 2C were similarly converted to promoter occupancy data shown **G**.

Fig. S5

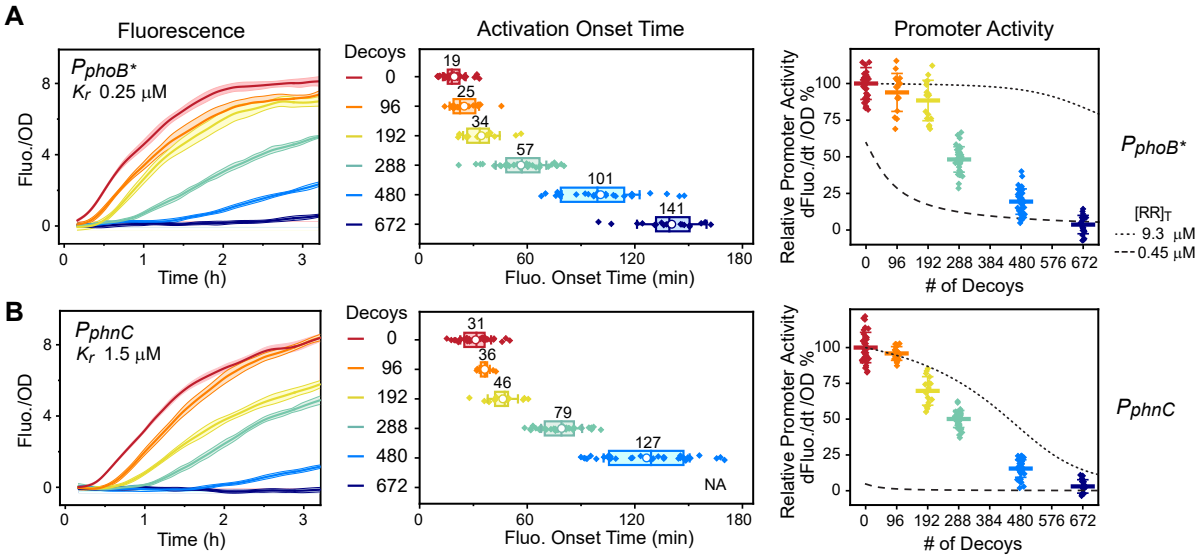

Figure S5. Effects of decoy sites on transcription output in the autoregulatory WT strains. Time courses of YFP reporter activation (*left*), activation onset time (*middle*) and relative steady promoter activities (*right*) are illustrated for P_{phoB*}-*yfp* (**A**) and P_{phnC}-*yfp* (**B**). RU2080 and RU1931 carrying different decoy plasmids were assayed for reporter fluorescence. Data from individual wells are shown by diamond symbols and the averages are shown in circles for onset times and horizontal bars for promoter activities. The data shown were from four independent experiments (except for 96 and 192 decoys with only two independent experiments) with eight individual cultures per experiment. Dashed and dotted lines (*right* panel) are the modeled curves with constitutive PhoB levels at indicated concentrations, which correspond to the WT $[RR]_T$ levels at non-stimulating and stimulating Pi conditions.

Fig. S6

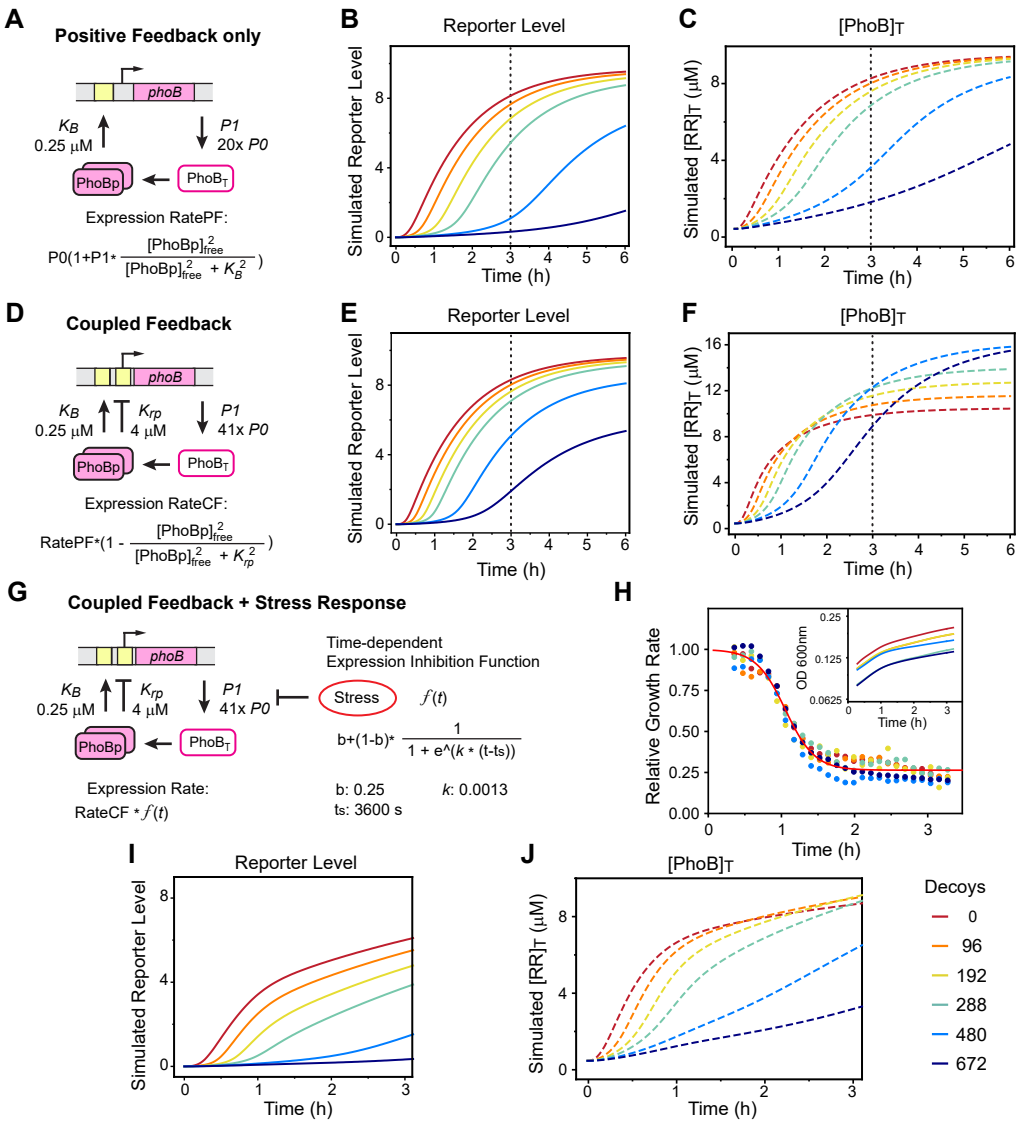

Figure S6. Simulated decoy effects in autoregulated systems. Three different schemes were modeled, including the autoregulated systems with only a positive feedback (**A-C**), with coupled positive and negative feedbacks (**D-F**), and coupled feedbacks plus repression by stress response (**G-J**). For each scheme, both reporter expression levels and total PhoB expression levels are shown. Vertical dotted lines correspond to 3 h after stimulation, an ending time point for experimental measurements. The most relevant parameters are indicated and the modeling details are described in supplementary materials. For a simple system with only a positive feedback (**A**), PhoB expression rate, RatePF, is dependent on occupation of the activation site with the binding affinity K_B as well as the basal and induced promoter strength parameters *P0* and *P1*. Increasing the number of decoy sites delays the reporter activation (**B**) and PhoB accumulation (**C**). For a coupled feedback system (**D**), PhoB expression rate RateCF contains a factor reflecting the binding of PhoBp to the repression site. The affinity to the repression site, K_{rp}, is much weaker than that to the activation site. Thus, the decoy titration effect is greater for the negative feedback than the positive feedback. Competition by decoys leads to less auto-repression and the model predicts higher PhoB expression levels with decoys than without decoys (**E** and **F**), which is not consistent with experimental observation. Response delay due to decoy titration is still non-trivial. It is known that Pi starvation promotes stress response thus the activation delay caused by decoys may be coupled with stress response to have a great impact on response. Stress response induced by Pi starvation involves complex pathways regulated RpoS and ppGpp thus are difficult to model. An extremely simplified transcription repression effect by stress response is considered in the third autoregulation scheme (**G**). A time-dependent stress repression function $f(t)$ is used to modify the PhoB expression rate. $f(t)$ is approximated using the stress-induced growth rate reduction obtained from OD measurements (**H**). For simplicity, it is assumed that stress-induced transcription repression has the same function as growth rate reduction. The half-time of stress-induced repression is estimated to be ~1 h. Simulated reporter levels and total PhoB concentrations are shown in (**I**) and (**J**). Decoys cause significant delay of PhoB accumulation into a starvation phase when stress-induced repression plays a major role in transcription regulation. This stress-related repression effect caused by response delay overshadows the transcription-increasing effect caused by decoy titration on the auto-repression site.

Fig. S7

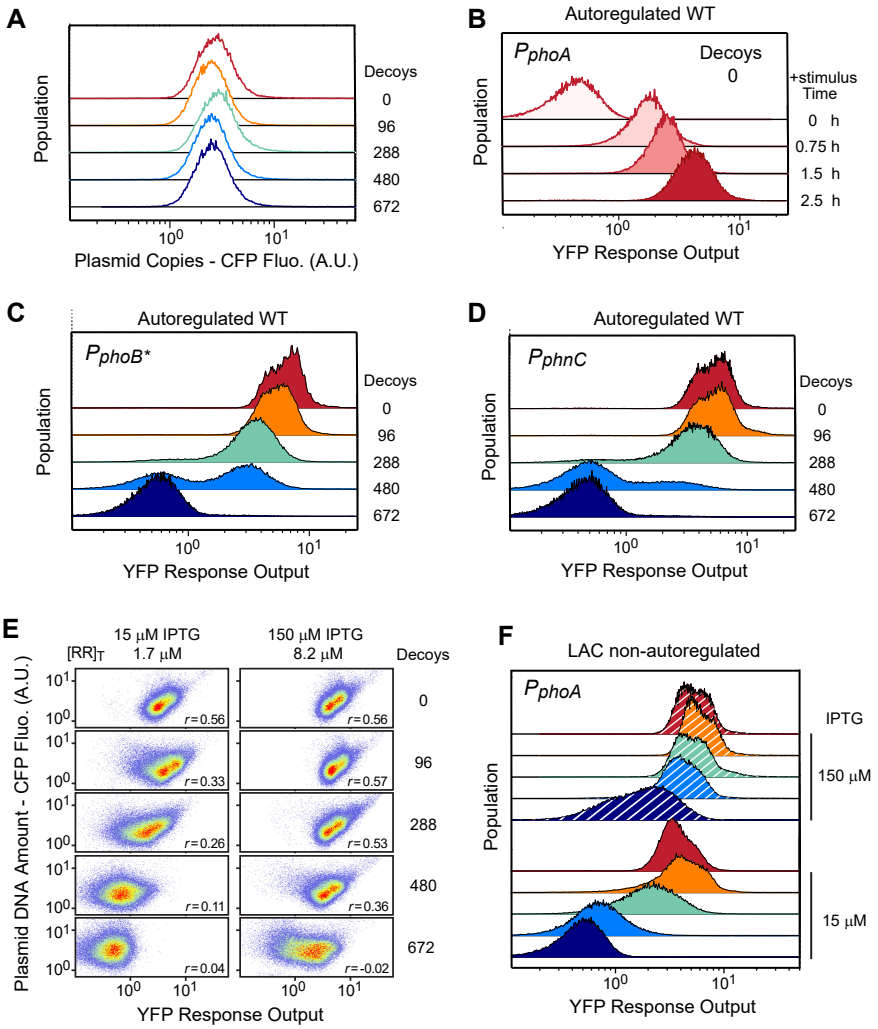

Figure S7. Flow cytometry analyses of reporter fluorescence population distribution. (**A**) Identical CFP fluorescence distribution for decoy plasmids. Histograms of CFP fluorescence were shown for strain RU2079 carrying pLH10, pRG491, pLH6, pLH8 and pLH9. (**B**) Gradual increase of P_{phoA}-*yfp* fluorescence in the absence of decoys during the time course of stimulation. YFP fluorescence of RU2079/pLH10 was measured by flow cytometry at indicated time after stimulation. (**C** and **D**) Bimodal distribution of reporter fluorescence for P_{phoB*}-*yfp* (**C**) and P_{phnC}-*yfp* (**D**). Histograms of YFP reporter fluorescence were shown for the autoregulated WT strains RU2080 and RU1931 carrying indicated number of decoy sites. (**E**) Flow cytometry density plots of single cell fluorescence for strain RU1988 (P_{phoA}-*yfp*) with decoys. IPTG concentrations of 15 μM (*left*) and 150 μM (*right*) were used to maintain two constant PhoB concentrations. The Spearman correlation coefficient *r* was calculated to evaluate the correlation between CFP and YFP fluorescence, reflecting the correlation between plasmid DNA amount and reporter response. (**F**) Graded reporter response in non-autoregulatory strains. Histograms of the YFP reporter fluorescence data from (**E**) indicate uni-modal distribution of reporter fluorescence output independent of the number of decoy sites or PhoB levels.

Table S1. Strains and plasmids used in this study.

Strains / plasmids	Relevant characteristics	Reference / source
Strains *E. coli*		
DH5α	General cloning strain	Invitrogen
BW25113	Wild-type, *lacI*^{q} *rrnB*$_{T14}$ Δ*lacZ*$_{WJ16}$ *hsdR514* Δ*araBA-D*$_{AH33}$ Δ*rhaBAD*$_{LD78}$	(10)
BW25141	*pir rrnB3* Δ*lacZ4787 hsdR514* DE(*araBAD*)567 DE(*rhaBAD*)568 Δ*phoBR580*	(11)
RU1616	LAC, Φ(Δ*phoBp* P$_{lac}$-*phoBR*) in BW25113	(5)
RU1988	*P$_{phoA}$-yfp,* LAC, *attHK::*pRG261 in RU1616	This study
RU1989	*P$_{phoB*}$-yfp,* LAC, *attHK::*pLH1 in RU1616	This study
RU1990	*P$_{phnC}$-yfp,* LAC, *attHK::*pLH2 in RU1616	This study
RU2079	*P$_{phoA}$-yfp,* WT, *attHK::*pRG261 in BW25113	This study
RU2080	*P$_{phoB*}$-yfp,* WT, *attHK::*pLH1 in BW25113	This study
RU1931	*P$_{phnC}$-yfp,* WT, *attHK::*pLH2 in BW25113	This study
Plasmids		
pAH69	Helper plasmid for CRIM integration, Ap^{r}	(11)
pCL1920	Control plasmid without fluorescence reporter, Sp^{r}	(12)
pRG261	*P$_{phoA}$-yfp* for CRIM integration, Sp^{r}	(13)
pRG368	*P$_{phoB*}$-yfp*, Sp^{r}	(2)
pRG400	*P$_{phnC}$-yfp*, Sp^{r}	This study
pLH1	*P$_{phoB*}$-yfp* for CRIM integration, Sp^{r}	This study
pLH2	*P$_{phnC}$-yfp* for CRIM integration, Sp^{r}	This study
pRG475	Golden Gate cloning vector, *P$_{tet}$-cfp*, Ap^{r}	This study
pLH10	0 PhoB binding site (~170 bp non-specific DNA) in pRG475, Ap^{r}	This study
pRG491	1 high affinity PhoB binding site in pRG475, Ap^{r}	This study
pRG492	2 high affinity PhoB binding site in pRG475, Ap^{r}	This study
pLH6	3 high affinity PhoB binding site in pRG475, Ap^{r}	This study
pLH8	5 high affinity PhoB binding site in pRG475, Ap^{r}	This study
pLH9	7 high affinity PhoB binding site in pRG475, Ap^{r}	This study

Table S2. Parameter values used in the model.

Reaction / Parameter	Value	Source
Phosphorylation cycle		
C_p	4.3 μM	(5)
C_t	0.8 μM	(5)
t_p	600 s	Estimated from Figure S1 of (2) [a]
DNA binding competition		
Binding affinities K_{DNA}		
K_r (P_{phoB*} *reporter)*	0.25 μM	(2)
K_r (P_{phoA} *reporter)*	0.6 μM	(1)
K_r (P_{phnC} *reporter)*	1.5 μM	(2) [b]
K_{decoy}	0.2 μM	Figure S1
K_B (*phoB* auto-activation site)	0.25 μM	(2)
K_{rp} (*phoB* auto-repression site)	4 μM	(2)
K_{en}	0.6 μM	Estimated [a]
DNA concentrations		
DNA_0 (one site)	1.66×10^{-3} μM	Estimated [a]
Decoy	N x DNA0	Figure S2
En0	54 x DNA0	Estimated [a]
Copy of genome equivalent	1.5	Estimated [a]
Protein concentrations		
PhoB (WT, Pi-replete)	0.45 μM	(1,5)
PhoB (WT, Pi-depleted)	9.45 μM	(1,5)
PhoB (LAC, 15 μM IPTG)	1.7 μM	(1,5)
PhoB (LAC, 150 μM IPTG)	8.2 μM	(1,5)
Autoregulation		
Protein dilution & degradation		
k_{dil}	2×10^{-4} s^{-1}	(2)
Protein production		
P_0	0.45 x k_{dil}	(2)
P1 (positive feedback only)	20 (x P_0)	(2)
P1 (coupled feedback)	41 (x P_0)	(2)
Stress repression function		
b	0.25	Figure S6
k	0.0013 s^{-1}	Figure S6
t_s	3600 s	Figure S6

a. See supplementary texts for details

b. EMSA data for *phnC* promoter DNA binding (2) were re-fitted with the free PhoBp concentration instead of the total PhoBp concentration to derive a K_D of 1.5 μM.

References

1. Gao, R. and Stock, A.M. (2015) Temporal hierarchy of gene expression mediated by transcription factor binding affinity and activation dynamics. *mBio*, **6**.

2. Gao, R. and Stock, A.M. (2018) Overcoming the cost of positive autoregulation by accelerating the response with a coupled negative feedback. *Cell Rep.*, **24**, 3061-3071.

3. Santos-Zavaleta, A., Sanchez-Perez, M., Salgado, H., Velazquez-Ramirez, D.A., Gama-Castro, S., Tierrafria, V.H., Busby, S.J.W., Aquino, P., Fang, X., Palsson, B.O. *et al.* (2018) A unified resource for transcriptional regulation in Escherichia coli K-12 incorporating high-throughput-generated binding data into RegulonDB version 10.0. *BMC Biol.*, **16**, 91.

4. Schmidt, A., Kochanowski, K., Vedelaar, S., Ahrne, E., Volkmer, B., Callipo, L., Knoops, K., Bauer, M., Aebersold, R. and Heinemann, M. (2016) The quantitative and condition-dependent *Escherichia coli* proteome. *Nat. Biotechnol.*, **34**, 104-110.

5. Gao, R. and Stock, A.M. (2013) Probing kinase and phosphatase activities of two-component systems *in vivo* with concentration-dependent phosphorylation profiling. *Proc. Natl. Acad. Sci. USA*, **110**, 672-677.

6. Yang, C., Huang, T.W., Wen, S.Y., Chang, C.Y., Tsai, S.F., Wu, W.F. and Chang, C.H. (2012) Genome-wide PhoB binding and gene expression profiles reveal the hierarchical gene regulatory network of phosphate starvation in *Escherichia coli*. *PLoS One*, **7**, e47314.

7. Bremer, H. and Dennis, P.P. (1996) In Neidhardt, F. C., Curtiss, R., III, Ingraham, J. L., Lin, E. C. C., Low, K. B., Magasanik, B., Reznikoff, W. S., Riley, M., Schaechter, M. and Umbarger, H. E. (eds.), *Escherichia coli and Salmonella: cellular and molecular biology*. ASM Press, Washington, DC, Vol. 2, pp. 1553-1569.

8. Gao, R., Godfrey, K.A., Sufian, M.A. and Stock, A.M. (2017) Counterbalancing regulation in response memory of a positively autoregulated two-component system. *J. Bacteriol.*, **199**.

9. Batchelor, E. and Goulian, M. (2003) Robustness and the cycle of phosphorylation and dephosphorylation in a two-component regulatory system. *Proc. Natl. Acad. Sci. USA*, **100**, 691-696.

10. Datsenko, K.A. and Wanner, B.L. (2000) One-step inactivation of chromosomal genes in *Escherichia coli* K-12 using PCR products. *Proc. Natl. Acad. Sci. USA*, **97**, 6640-6645.

11. Haldimann, A. and Wanner, B.L. (2001) Conditional-replication, integration, excision, and retrieval plasmid-host systems for gene structure-function studies of bacteria. *J. Bacteriol.*, **183**, 6384-6393.

12. Lerner, C.G. and Inouye, M. (1990) Low copy number plasmids for regulated low-level expression of cloned genes in *Escherichia coli* with blue/white insert screening capability. *Nucleic Acids Res.*, **18**, 4631.

13. Gao, R. and Stock, A.M. (2013) Evolutionary tuning of protein expression levels of a positively autoregulated two-component system. *PLoS Genet.*, **9**, e1003927.